

Astrometric Errors Introduced by Interpixel Capacitive Coupling in Hybridized Arrays

Kevan Donlon^a, Zoran Ninkov^a, Stefi Baum^{a,b}

^aRochester Institute of Technology, Chester F. Carlson Center for Imaging Science, 54 Lomb Memorial Drive, Rochester, New York, 14623

^bUniversity of Manitoba, Department of Physics and Astronomy, 66 Chancellors Cir, Winnipeg, MB, Canada

Abstract. Interpixel capacitance (IPC) between adjacent pixels in hybridized arrays gives rise to an electrostatic cross talk. This cross talk causes MTF degradation and blurring of images or spectra collected using these devices. As pixel size is driven down from the 18 micron pixel pitch of the H2RG read out circuits to the 10 or 15 micron H4RGs IPC is driven up resulting in greater cross talk, all else being equal. Mounting evidence indicates that IPC varies as a function of depletion state of the photo-active diodes. For single pixel events, increasing the event intensity corresponds to a decreasing fractional coupling. If left uncorrected, IPC can give rise to systematic errors in precision astrometric and photometric measurements, in particular when dealing with confused point sources or spatially extended structures for shape measurements as demonstrated through comparison of registered sources from ESO HAWK-I and HST ACS WFC datasets. Furthermore these errors will be the most significant when operating near the sensitivity limit of these devices. Deconvolution based correction methods are invalidated by this same signal dependence. Instead a numerical method of successive approximation can be used to correct coupling due to a well characterized IPC. Examination of single pixel reset data above flat fields could be used to characterize IPC's functional relationship for neighboring pixels. This higher quality characterization can result in more accurate correction.

Keywords: Interpixel Capacitance, IPC, Hybridized HgCdTe, Cross Talk, Single Pixel Reset, H2RG, Deconvolution.

Address all correspondence to: Kevan Donlon, Rochester Institute of Technology, Chester F. Carlson Center for Imaging Science, 54 Lomb Memorial Drive, Rochester, New York, 14623; E-mail: KevanADonlon@gmail.com

Hybridized detector arrays are composed of three distinct regions: a photo-sensitive layer, a read-out circuit (ROIC) layer, and an indium bump bond layer responsible for connecting the two. This detector design divorces the read-out electronics from the light detection which allows for unconventional materials or detection techniques to be used without disrupting the proven technology in the ROIC.¹

The introduction of an intermediate layer that supports the presence of electric fields gives rise to a conventional capacitor; conductive materials separated by a dielectric epoxy. This parasitic electrostatic connection causes the electronic state of a single pixel to impact not just the readout node that corresponds to that pixel, but also the read-out node corresponding to nearby pixels^{2,3}. In addition to this conventional capacitor, electric fields from the depletion region of the photodiodes

34 bleed out into the bump bond layer^{2,4} These fringing fields vary non-linearly as a diode is ex-
 35 posed to photons^{5,6,4} This non-linear field strength results in a non-uniform capacitance between
 36 neighboring pixels as their depletion region changes size.

The impact that this capacitance has on an output image, $O(i, j)$, has historically been formal-
 ized as convolution of an input image, $I(i, j)$, with a nearest neighbor coupling kernel, $K(i, j)$.⁷
 The coupling coefficient, α , indicates the fractional signal collected on a single pixel that manifests
 on the output of each neighboring pixel.

$$K(i, j) = \begin{pmatrix} 0 & \alpha & 0 \\ \alpha & 1 - 4\alpha & \alpha \\ 0 & \alpha & 0 \end{pmatrix} \quad (1)$$

$$O(i, j) = K(i, j) * I(i, j) \quad (2)$$

A non-uniform capacitance results in a non-uniform coupling coefficient. Due to the fringing
 fields from the photo-diodes, IPC varies as a function of photons collected in the neighborhood of
 readout node.⁴ Only giving consideration to the final image output, coupling between two pixels
 varies as a function of the level of each pixel. This gives rise to a systems of equations where S
 is the uncoupled incident level of the central pixel, B is the background signal, N is the readout
 value of the neighboring pixel, and C is the readout value of the central pixel and α is the fractional
 coupling coefficient.

$$C = S - 4\alpha S + 4\alpha B \quad (3)$$

$$N = B + \alpha S - \alpha B \quad (4)$$

Solved for α this yields:

$$\alpha = \frac{N - B}{C + 4N - 5B} \quad (5)$$

37 Using this convention, $\alpha = \alpha(S, B)$. Within this work, a method to characterize this coupling is
38 discussed, a technique for correcting a well characterized coupling is referenced and applied to
39 data for the scientific ramifications to be assessed. The domain of these parameters is intentionally
40 left ambiguous. All values can be taken in the charge domain, the voltage domain, or any arbitrarily
41 defined continuous injective mapping over the charge domain. The key facet, is that the domain
42 must be consistent and must match the domain for the coupling coefficient. The particular func-
43 tional behavior of α will be distinct if given in terms of Q or V , but the preceding equations and
44 the conclusions that follow will hold in any particular instance of this general approach.

45 **1 IPC and systematic errors**

46 Characterization of the coupling in isolation can aid in understanding the nature of the measure-
47 ment tool and the systematic errors that it can introduce, but perhaps more valuably when that
48 error behaves deterministically rather than stochastically, its impact on scientific data in particular
49 circumstances can be elucidated and corrected. Previous work has made an effort to predict the
50 impact that IPC can have on scientific data when examining crowded fields;¹⁰ here those predic-
51 tions will be empirically verified. With a well characterized coupling coefficient, the effect of IPC
52 can be backed out using the following iterative method¹⁰ with S , C , and α as used in equations 3
53 to 5, q indicating iteration count, and m , n , i , and j indicating spatial pixel indexes:

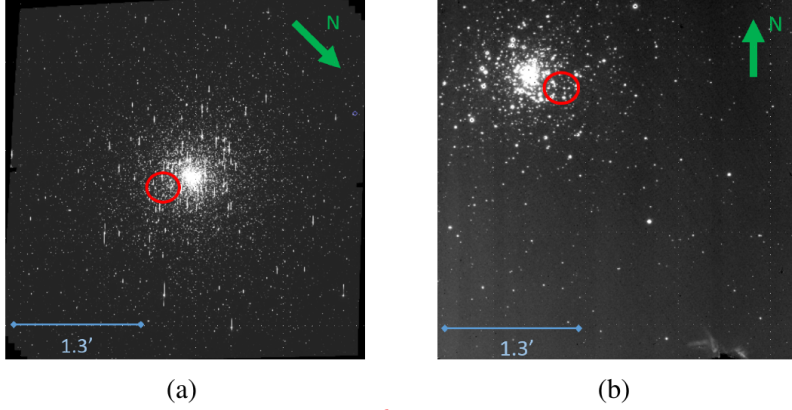


Fig 1: NGC1851 (Cladwell 73). Located at $05^h 14^m 07^s$, $-40^\circ 02' 48''$. Red circle indicates region of interest where the binary is located. (a) MAST provided HST ACS WFC observation. (b) ESO provided HAWK-I 2.0-2.3 μm observation

$$\hat{S}_q(i, j) = C(i, j) - \sum_{m=i-1}^{i+1} \sum_{n=j-1}^{j+1} \left[\alpha \left(\hat{S}_{q-1}(i, j), \hat{S}_{q-1}(m, n) \right) \cdot \hat{S}_{q-1}(m, n) \right] + \sum_{m=i-1}^{i+1} \sum_{n=j-1}^{j+1} \left[\alpha \left(\hat{S}_{q-1}(m, n), \hat{S}_{q-1}(i, j) \right) \cdot \hat{S}_{q-1}(i, j) \right] \quad (6)$$

$$\hat{S}_0(a, b) = C(a, b) \quad (7)$$

54 Here we will examine a resolvable binary source pair that has been observed by both the Euro-
55 pean Southern Observatory (ESO) instrument HAWK-I's hybridized H2RG HgCdTe $2.5\mu m$ array
56 at the Very Large Telescope (VLT) and the CCD array of the Hubble Space Telescope's (HST)
57 Advanced Camera for Surveys (ACS) Wide Field Camera (WFC). The first binary explored here is
58 located on the western side of NGC1851 with full frames shown in figure 1 and the particular bi-
59 nary shown in figure 2. It was selected for a number of reasons. It is sufficiently above background
60 in the HAWK-I exposure to be clearly visible. The sources are visibly resolvable but extremely
61 confused in the IR image as illustrated in figure 3. It was sufficiently below saturation in the HST
62 image that minimal blooming occurs.

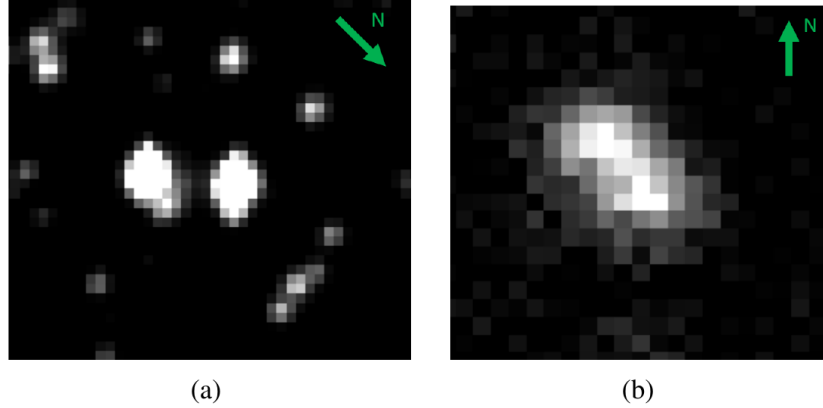


Fig 2: Binary of interest. (a) MAST provided HST ACS WFC observation. (b) ESO provided HAWK-I 2.0-2.3 μm observation.

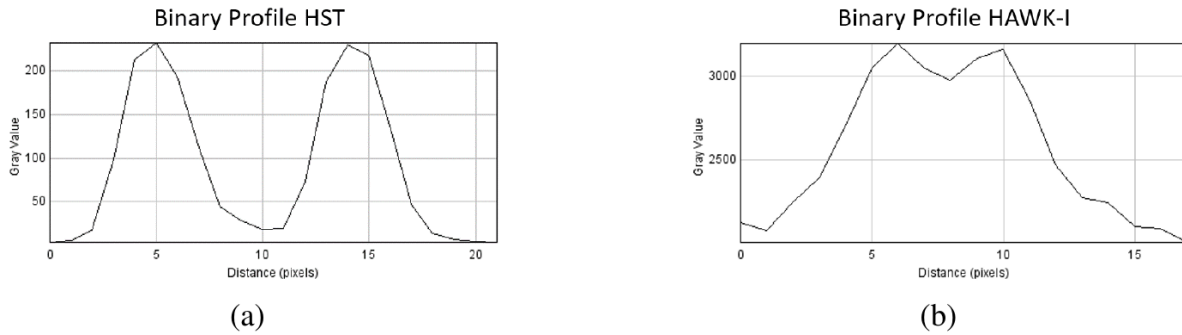


Fig 3: Profile across the binary in pixel space. Little confusion in HST image but significant region of overlap in HAWK-I image. Images have distinct pixel scales. (a) HST (b) HAWK-I

63 Point spread fitting using the python photutils implementation¹¹ of DAOPhot¹² was performed
 64 to estimate the angular separation between the binary in the Hubble frame as well as the HAWK-I
 65 frame. Theoretical predictions indicate that in arrays with IPC present, the separation between
 66 confused sources will be underestimated.¹⁰ This is due to the signal dependence of IPC causing
 67 preferential blurring towards the center of the binary compared to away. IPC has been characterized
 68 as a function of signal strength using hot pixels present in dark exposures of the HAWK-I device
 69 as shown in figure 4.

70 This characterization will then be used to decouple the HAWK-I image. Comparisons between
 71 the point spread fits from the original HAWK-I frame, the corrected HAWK-I frame, and the
 72 Hubble frame are shown in the following table. The fit from the Hubble frame will be used as a

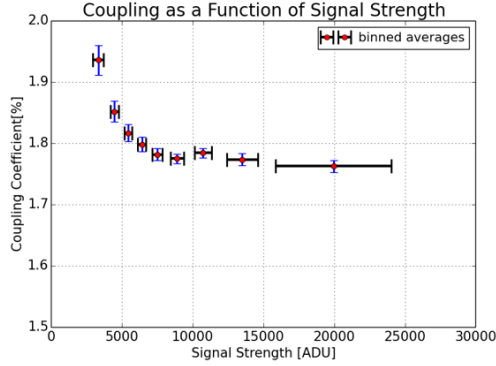


Fig 4: Estimate of $\alpha(S)$ using hot pixels as isolated single pixel events above a dark background. The form is the same as has been historically observed in this type of detector. Coupling peaks on the order of 2.00% tapering down to 1.75%. Vertical error bars indicate 98% confidence on the means. Horizontal error bars indicate $\pm 1\sigma$ bounds on mean signal level binning.

73 type of fiducial, as there is no IPC present and astrometric errors will be considered as deviation
 74 from this data.

	HST	HAWK-I, uncorrected	HAWK-I, IPC corrected
Separation [pix]	9.265	4.288	4.320
75 Separation [marcsec]	463.251 ± 0.583	456.363 ± 3.149	459.823 ± 3.149
Error [marcsec]	—	-6.888 ± 3.203	-3.428 ± 3.203
Error [%]	—	-1.48%	-0.74%

76 Separation of this confused binary using PSF fitting is measured to be smaller using data from
 77 a hybridized array compared to data from a CCD array. This underestimate is partially mitigated
 78 by correction using a partially characterized coupling coefficient. It is worth noting that part of this
 79 precision comes from the underlying geometric distortions incident on the Hubble and HAWK ar-
 80 rays. Raw HST images are anticipated to have up to 7% geometric errors but these field distortions
 81 are corrected to less than 0.5 *marcsecs* by using the AstroDrizzle preprocessing technique.¹⁴ On
 82 the VL 8m telescope the field correction is a more difficult problem as the IPC correction must be
 83 applied prior to any geometric correction. As a result the raw uncorrected data was examined here.

84 This raw frame includes an expected residual error on the visual field on the order of 35 marcsec .
85 However, this isn't the error that we care about for separation fitting. We need not be concerned
86 with overall flatness of the field but only local flatness over a small neighborhood of $\sim 25 \text{ pixels}$.
87 Examining the residuals presented in Libralto M, et al¹³ indicates that astrometric accuracy across
88 the field varies continuously with greater local change in residual error from distortions near the
89 edge of the frame. With a total astrometric error of $\pm 250 \text{ marcsecs}$ indicating an average per
90 pixel change in geometric accuracy on the order of 0.0625 marcsecs . These same residuals in-
91 dicate that the peak distortion can be seen to be approximately double this average; a maximum
92 per pixel change of 0.125 marcsecs . Extending that over the 25 pixel range, the maximum radius
93 for confusion of pointspreads presented in this work, a maximum expected impact on separation
94 of the geometric distortions on the order of 3.2 marcsecs . The geometric distortion's contribution
95 to separation error here is small. This is prior to any geometric field correction, the application
96 of a relatively simple 5th order polynomial type correction¹³ is a possibility but has not been used
97 on the data presented here. Using IPC correction that accounts for a change in coupling across
98 the field reduces the magnitude of this underestimate from 1.48% to 0.74%. This correction only
99 used a signal dependent characterization of IPC from hot pixels; it did not account for variation of
100 IPC across the neighboring pixel level as well. It is anticipated that a more complete characteri-
101 zation, such as that discussed later in this work, would allow for greater restoration of astrometric
102 accuracy.

103 *1.1 Sets of binaries*

104 In addition to the NGC1851 data, another object, an open cluster NGC3603 located at $11^h 15^m 23^s$,
105 $-61^\circ 15' 00''$ was examined to increase the number of binaries. The PSFs established from this

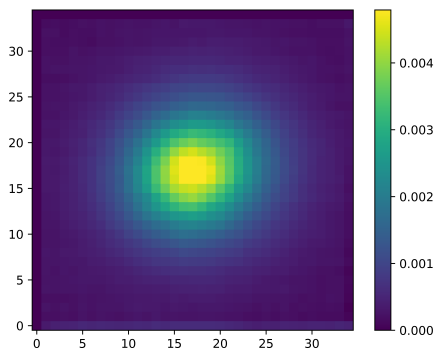


Fig 5: Constructed PSF from the NGC3603 frame for the HAWK-I array; raw and coupled are visually non-distinct.

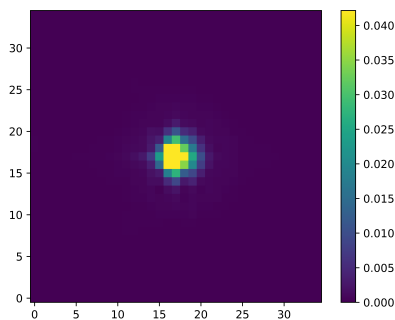


Fig 6: Constructed PSF from the NGC3603 frame for the HST array

106 frame are presented in figure 5 and 6. This same data is also illustrated as PSF cross sections
 107 in figures 7 and 8. This illustrates that the deconvolution impacts the measured PSFs in the an-
 108 ticipated way, by narrowing the FWHM and increasing energy in the peak. The FWHM of the
 109 PSF from the NGC3603 frame is substantially larger ($\sim 11 \text{ pixels} \approx 1.166 \text{ arcsec}$) than from
 110 the NGC1851 frame ($\sim 4 \text{ pixels} \approx 0.424 \text{ arcsec}$) due to introduction of an adaptive optic system
 111 between the two observations. The absence of this adaptive optic system is helpful when looking
 112 for confused sources, as a greater angular separation can give rise to the same degree of confusion.
 113 The NGC3603 has resulted in 74 binary stars being fit. These are characterized by the difference
 114 in measurement of angular separation between HAWK-I and HST.

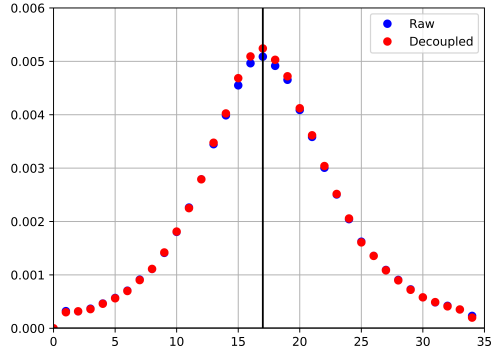


Fig 7: Constructed PSF cross section from the NGC3603 frame for the HAWK-I array. Note the higher peak for the decoupled PSF compared to the raw. Y-axis in units of fractional energy in pixel. X-axis in units of pixels

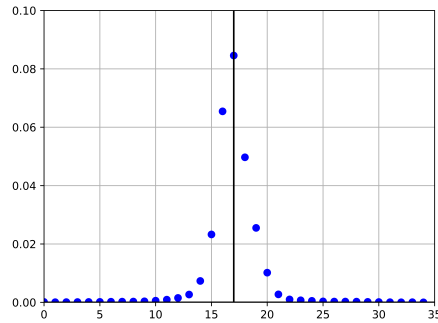


Fig 8: Constructed PSF cross section from the NGC3603 frame for the HST array. Y-axis in units of fractional energy in pixel. X-axis in units of pixels

115 Figure 9 illustrates a systematic decrease in separation error as a result of deconvolution of up
 116 to $8 \text{ } \textit{marcsec}$ with an average restoration on the order of $3.63 \text{ } \textit{marcsec}$. This lack of complete
 117 correction is likely due to the lack of complete characterization of the coupling coefficient. More
 118 importantly, this figure shows that IPC will introduce a systematic error in astrometry on the order
 119 of tens of $\textit{marcsec}$. The greatest error occurs when the confusion is greatest and drops to zero
 120 when the sources are no-longer confused. The data presented here is akin to and gives empirical
 121 validation to that simulated in previous work¹⁰ but does not have a clearly specified relationship
 122 between the relative intensities of the two sources or an absolutely defined peak intensity. That is to

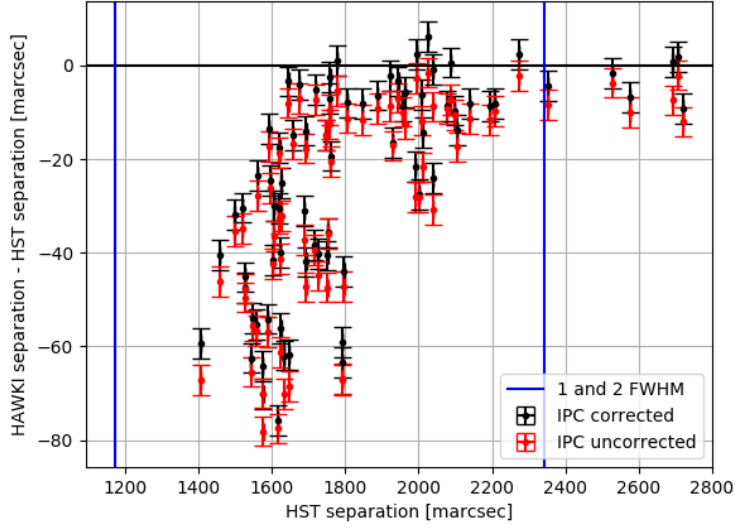


Fig 9: Error in separation from binary stars as a function of separation distance for corrected and uncorrected images of NGC3603. 74 stars are examined here. The corrected data systematically increases the separation returned from PSF fitting. In 72 of 74 cases, this resulted in a decrease in error relative to the uncorrected fit. In the two excepting cases the deconvolution pushed the estimate of separation from a small underestimate to a small overestimate.

123 say that this data is sampling from higher dimensional curves in both absolute and relative bright-
 124 ness. The dropoff in separation error as confusion of the sources decreases is clear; separation
 125 trends to nearly no astrometric error compared to the hubble data when the sources are distinct.

126 **2 Characterization using single pixel resets**

127 The technique applied in section one of this paper is preferable serves to mitigate the impact of
 128 IPC coupling on astrometric error but does not eliminate it completely. This is largely due to the
 129 assumption inherent to using hot pixel characterization. Hot pixels only provide a cross section
 130 through equation 5 where $\alpha(S|B = 0)$ rather than the full $\alpha(S, B)$. What follows outlines a
 131 method of using single pixel resets to characterize IPC more accurately over a more representative
 132 domain. This higher quality characterization feeds into a more accurate correction, yielding further
 133 minimization of astrometric errors.

134 In order to characterize the coupling coefficient, single pixel events can be examined.⁸ Hot
 135 pixels over dark frames are an effective technique to characterize IPC coupling as a function of
 136 signal level but cannot explore the dependence on the depletion state of the neighboring pixels⁶ ,
 137 as in order to be an isolated event in a dark frame, the neighbor level must be approximately zero. A
 138 proposed alternative method is to use single pixel resets. These hybridized arrays allow for pixels
 139 to be addressed and reset individually. Extending the technique of SPR to a full characterization
 140 can be done through the following method:

- 141 1. Reset the array to prepare for an exposure.
- 142 2. Expose the array to a flat field for to produce a particular background level.
- 143 3. Reset isolated pixels using a voltage V_{sig} corresponding to a particular level of depletion here
 144 called 'signal'.
- 145 4. Read out the array and repeat for new V_{sig} and/or exposure time.

146 A sample for this type of data can be seen in figure 10. Considering only nearest neighbor coupling,
 147 each frame obtained using this method where n isolated pixels are reset with a center-to-center
 148 gridded separation of m pixels in a square grid you acquire n samples of your C value, $4n$ samples
 149 of your N value, and $(m^2 - 5)n$ samples of your B value. These sample counts are what will limit
 150 statistical confidence on results. Instances of each of these data types are illustrated in figure 10b.

From this type of frame a scatter of points can be built up using:

$$\langle \alpha \rangle = \frac{\langle N \rangle - MED(B)}{\langle C \rangle + 4\langle N \rangle - 5(MED(B))} \quad (8)$$

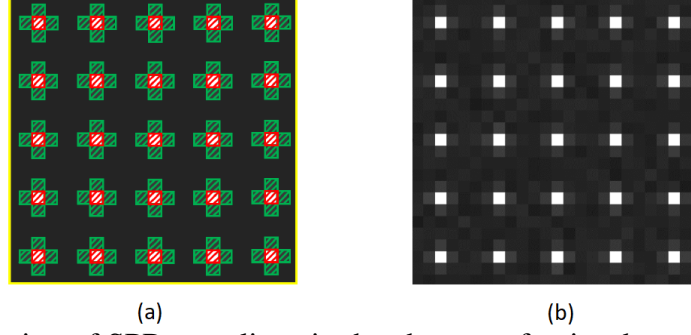


Fig 10: (a) An illustration of SPR samplings in the absence of noise demonstrating the four sorts of pixel contained. Red pixels are instances of C , green are instances of N , all others are instances of B . (b) sample SPR frame with IPC, shot noise on the background, and read noise.

Where $MED(B)$ is the median of the set of B samples and $\langle X \rangle$ indicates the mean of the set of samples of X and with expected noise statistics governed by:⁹

$$\sigma_\alpha^2 \approx \vec{J} \Sigma \vec{x} \vec{J}^T \quad (9)$$

$$\sigma_\alpha^2 \approx \frac{((C) - \langle B \rangle)^2 \sigma_N^2 + (\langle N \rangle - \langle C \rangle)^2 \sigma_B^2 + (\langle N \rangle - \langle B \rangle)^2 \sigma_C^2 + 2((C) - \langle B \rangle)(\langle N \rangle - \langle C \rangle) \sigma_{N,B} + 2((C) - \langle B \rangle)(\langle N \rangle - \langle B \rangle) \sigma_{N,C} + 2(\langle N \rangle - \langle C \rangle)(\langle N \rangle - \langle B \rangle) \sigma_{B,C}}{((C) + 4\langle N \rangle - 5\langle B \rangle)^4} \quad (10)$$

Sensibly, this noise blows up when $C \approx B$, as the read out does not indicate a uniquely defined coupling coefficient in this circumstance. In order to characterize the coupling coefficient in this neighborhood, interpolation must be used. To examine the behavior of this technique, it has been applied to simulated data with a known coupling coefficient prescribed and applied. The form used for this simulated coupling coefficient was as follows:

$$\alpha(S, B) = A_0 \exp\left(-\frac{|S - B|}{k_0}\right) + A_1 \exp\left(-\frac{(S^2 + B^2)^{0.5}}{k_1}\right) + \alpha_\infty \quad (11)$$

151 This form is approximate but is informed by observations⁵ and simulations⁴ as well as constraining

152 that the coupling coefficient from pixel i to j is identical to the coupling coefficient from pixel j to

153 i .

154 These simulated frames were created using the following method:

- 155 1. Generate a uniform background level.
- 156 2. Apply shot noise to each sample of background level.
- 157 3. Set fixed pixels to a reset level.
- 158 4. Simulate IPC coupling through application of equation 2 with coupling defined by equa-
159 tion 11
- 160 5. Apply zero-mean normal read noise to each sample.
- 161 6. Repeat for many background and reset levels.

162 This technique preserves the property of IPC that signal and shot noise are coupled, but read
163 noise is not. Every reset, through equation 8 gives rise to an observation of $(\alpha|S, B)$. Assem-
164 bling all this data yields a scatter plot in three dimensions. A simulated dataset was examined by
165 processing 100 frames at each point noted in 11 a with each frame containing 9,604 resets with
166 30RMS simulated read noise. Fitting this data to the prescribed form yields coefficients and errors
167 summarized in the following table.

Parameter	Input	Estimate	Fractional Error
A_0	0.400[%]	0.416[%]	+0.040
A_1	0.400[%]	0.375[%]	-0.063
α_∞	0.650[%]	0.644[%]	-0.009
k_0	20,000 [e-]	15,573 [e-]	-0.221
k_1	28,284 [e-]	30,816 [e-]	-0.090

168

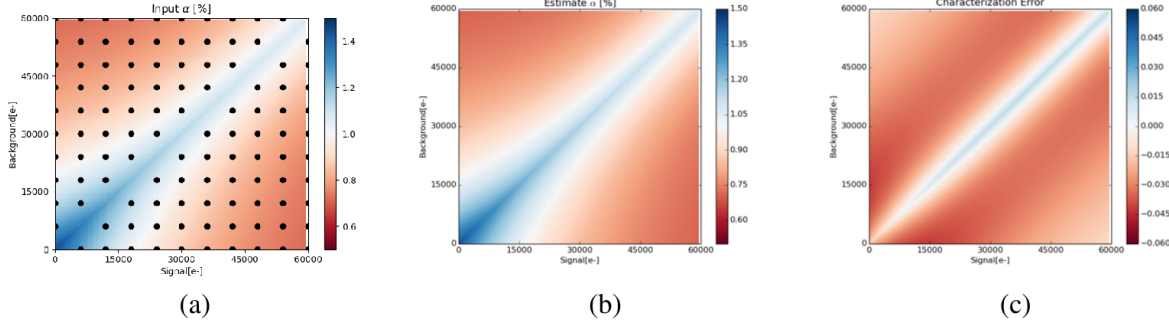


Fig 11: (a) Input $\alpha(S, B)$ as prescribed by equation 11 with sampled frames collected at the illustrated points. Note that no frames were examined where $S = B$ due to the non-uniqueness of equation 11 at those points. (b) Regressed form of $\alpha(S, B)$ using data frames described to fit to equation 11. (c) Difference between (b) and (a) $Regressed - Input$. Peak overestimate in α of 0.020[%] and peak underestimate of 0.045[%].

169 Though the error on any individual parameter can be quite large, the errors compensate for each
 170 other yielding a maximum overestimate in fractional IPC of 0.02[%] and maximum underestimate
 171 of 0.045[%] for coupling scaling from 0.65[%] to 1.45[%].

172 The behavior of this fit is illustrated in figure 11b with figure 11c showing the difference be-
 173 tween the input coupling and the regressed coupling as a function of S and B .

174 3 Summary

175 A particular set of binaries is examined where the impact of IPC on separation estimates is indi-
 176 cated to be significant. PSF fitting techniques corroborate this claim when compared to fiducial
 177 data from HST. Correction of IPC using a partial hot pixel based characterization of the coupling
 178 coefficient is performed. The corrected data exhibits a smaller underestimate of separation indicat-
 179 ing incomplete restoration of astrometric accuracy. A technique by which IPC can be characterized
 180 as a function of pixel and background level using single pixel resets is explored. The noise behavior
 181 and statistical properties of this type of characterization are explored using simulated data.

182 When examining dense fields, where sources are not well isolated, PSF fitting is the dominant

183 technique to obtain astrometric and photometric measurements. IPC causes distortions to the PSF
184 as the signal integrated on a pixel changes; bright sources appear more narrow than faint sources.
185 Furthermore, when the sources are significantly confused, the PSFs distort asymmetrically. This
186 work shows that these distortions can cause inaccuracy of astrometric measurements as well as
187 demonstrates partial success of a correction algorithm when using a partial characterization of
188 IPC. Future work will explore this error more systematically on sets of binaries to establish trends
189 and better inform astronomers of the degree to which IPC will impact their measurements for
190 particular observations.

191 *Acknowledgments*

192 We would like to thank NASA for providing support and funding through contract NAS5-02105.
193 Some of the data presented in this paper were obtained from the Mikulski Archive for Space
194 Telescopes (MAST). STScI is operated by the Association of Universities for Research in Astron-
195 omy, Inc., under NASA contract NAS5-26555. Based on observations made with the NASA/ESA
196 Hubble Space Telescope, and obtained from the Hubble Legacy Archive, which is a collabora-
197 tion between the Space Telescope Science Institute (STScI/NASA), the European Space Agency
198 (ST-ECF/ESAC/ESA) and the Canadian Astronomy Data Centre (CADM/NRC/CSA). Based on
199 data obtained from the ESO Science Archive Facility under request numbers Donlok 321673 and
200 Donlok 321674.

201 *References*

202 1 A. Rogalski, K. Adamiec, and J. Rutkowski, *Narrow-Gap Semiconductor Photodiodes*, SPIE
203 Publications, Bellingham Washington (2000).

- 204 2 A. C. Moore, Z. Ninkov, and W. J. Forrest, “Quantum efficiency overestimation and deter-
205 ministic cross talk resulting from interpixel capacitance,” *Opt. Eng.* **45**, 076402 (2006).
- 206 3 H. C. Ohanian, *Classical Electrodynamics*, Infinity Science Press, Hingham Massachusetts,
207 2 ed. (2007).
- 208 4 K. Donlon, Z. Ninkov, S. Baum, and L. Cheng, “Modeling of hybridized infrared arrays for
209 characterization of interpixel capacitive coupling,” *Optical Engineering* **56** (2017).
- 210 5 L. Cheng, “Interpixel capacitive coupling,” Master’s thesis, Rochester Institute of Technology
211 (2009).
- 212 6 K. Donlon, Z. Ninkov, and S. Baum, “Signal dependence of inter-pixel capacitance in hy-
213 bridized HgCdTe H2RG arrays for use in James Webb space telescope’s NIRcam,” in *High*
214 *Energy Optical and Infrared Detectors for Astronomy VII*, A. D. Holland and J. Beletic, Eds.,
215 *Proc. SPIE* **9915** (2016).
- 216 7 A. C. Moore, Z. Ninkov, and W. J. Forrest, “Interpixel capacitance in non-destructive fo-
217 cal plane arrays,” in *Focal Plane Arrays for Space Telescopes*, T. J. Grycewicz and C. R.
218 McCreight, Eds., *Proc. SPIE* **5167**, 204–215 (2004).
- 219 8 S. Seshadri, D. M. Cole, B. R. Hancock, and R. M. Smith, “Mapping electrical crosstalk in
220 pixelated sensor arrays,” in *High Energy, Optical, and Infrared Detectors for Astronomy III*,
221 *Proc. SPIE* **7021** (2008).
- 222 9 H. H. Ku, “Notes on the use of propagation of error formulas,” *National Bureau of Standards*
223 **70C**, 263 (1966).
- 224 10 K. Donlon, Z. Ninkov, and S. Baum, “Point-spread function ramifications and deconvolution

- 225 of a signal dependent blur kernel due to interpixel capacitive coupling,” *Publications of the*
226 *Astronomical Society of the Pacific* **130** (2018).
- 227 11 L. Bradley, B. Sipocz, T. Robitaille, and E. T. et al., “astropy/photutils:v0.3,” (2016).
- 228 12 P. B. Stetson, “DAOPHOT - a computer program for crowded-field stellar photometry,” *Pub-*
229 *lications of the Astronomical Society of the Pacific* **99**, 191–222 (1987).
- 230 13 M. Libralato, A. Bellini, L. R. Bedin, G. Piotto, I. Platais, M. Kissler-Patig, and A. P.
231 Milone, “Ground-based astrometry with wide field imagers v. application to near-infrared
232 detectors:HAWK-I@VLT/ESO,” *Astronomy and Astrophysics* **563** (2014).
- 233 14 V. Kozhurina-Platais, N. Grogin, and E. Sabbi, “Accuracy of the HST standard astromet-
234 ric catalogs w.r.t. gaia,” Tech. Rep. ACS/WFC 2018-01, Space Telescope Science Institute
235 (2018).
- 236 15 K. Donlon, Z. Ninkov, and S. Baum, “Signal dependent interpixel capacitance in hybridized
237 arrays: simulation, characterization, and correction,” in *High Energy Optical and Infrared*
238 *Detectors for Astronomy VIII*, A. D. Holland and J. Beletic, Eds., *Proc. SPIE* **10709** (2018).